ACS APPLIED MATERIALS & INTERFACES

Research Article

www.acsami.org

Defect-Related Luminescent Mesoporous Silica Nanoparticles Employed for Novel Detectable Nanocarrier

Kun Ge,[†,‡,§] Cuimiao Zhang,[†,‡] Guang Jia,[*,‡] Huihui Ren,[‡] Jianyuan Wang,[‡] Aaron Tan,[⊥] Xing-Jie Liang,[*,∥] Aimin Zang,[§] and Jinchao Zhang[*,‡]

[‡]Key Laboratory of Chemical Biology of Hebei Province, Key Laboratory of Medicinal Chemistry and Molecular Diagnosis of the Ministry of Education, College of Chemistry & Environmental Science, Hebei University, Baoding 071002, P. R. China

[§]Affiliated Hospital of Hebei University, Baoding 071000, P. R. China

[⊥]Research Department of Nanotechnology, UCL Division of Surgery & Interventional Science, UCL Medical School, University College London (UCL), London NW3 2QG, United Kingdom

[∥]CAS Key Lab of Nanomaterials Bioeffects and Nanosafety, National Center for Nanoscience and Technology of China, Beijing 100190, P. R. China

Supporting Information

ABSTRACT: Uniform and well-dispersed walnut kernel-like mesoporous silica nanoparticles (MSNs) with diameters about 100 nm have been synthesized by a templating sol−gel route. After an annealing process, the as-obtained sample (DLMSNs) inherits the well-defined morphology and good dispersion of MSNs, and exhibits bright white-blue luminescence, higher specific surface area and pore volume, and better biocompatibility. The drug loading and release profiles show that DLMSNs have high drug loading capacity, and exhibit an initial burst release followed by a slow sustained release process. Interestingly, the luminescence intensity of the DLMSNs-DOX system increases gradually with the increase of cumulative released DOX, which can be verified by the confocal laser scanning images. The drug carrier DLMSNs can potentially be applied as a luminescent probe for monitoring the drug release process. Moreover, the DLMSNs-DOX system exhibits potent anticancer effect against three kinds of cancer cells (HeLa, MCF-7, and A549 cells).

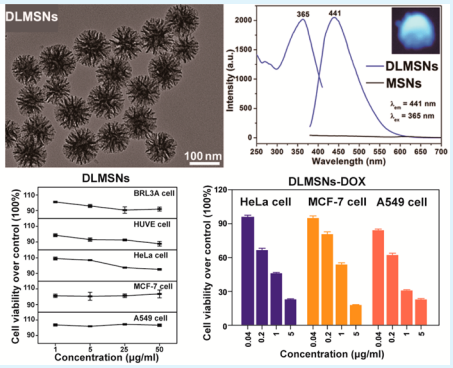

KEYWORDS: *mesoporous silica nanoparticles, defect-related luminescence, drug carrier, anticancer effect*

INTRODUCTION

In the past few years, novel drug delivery systems (DDS) have gained much attention because of their greater efficacy and safety, enhanced bioavailability, controllable release profile, and predictable therapeutic response.[1−7] An ideal drug carrier generally possesses some properties, such as appropriate particle size distribution, good biocompatibility, targeting ability, and controlled drug release manner.[8,9] Moreover, an efficient drug delivery system should exhibit rational toxicity and keep the optimum drug concentration in the tissues, which can realize efficient therapy while reducing toxicity.[6,10] The system toxicity has been considered the major adverse side effects of the traditional chemotherapy drugs, which could not distinguish healthy and diseased cells.[11] Therefore, high-fidelity drug carriers are desired for the applications of anticancer drugs in cancer therapy.[12,13]

Currently, various types of inorganic and organic nanomaterials have been employed for drug carriers. Among them, mesoporous silica nanoparticles have been developed as robust inorganic scaffolds for the delivery of drugs because of their distinctive characteristics, such as high drug loading capacity, favorable biocompatibility, and a relative ease for surface functionalization.[1,14−20] Although the preparation of MSNs with diverse morphologies has been extensively investigated, the synthesis of monodisperse MSNs with smaller particle size remains a challenge. In particular, the synthesis of MSNs smaller than 200 nm attracts significant interest, which may potentially applied in fields of DDS, cell imaging, and disease diagnosis. Furthermore, it was also reported that the luminescent mesoporous materials had potential applications in drug delivery and disease therapy.[6,21,22] These DDS not only possess high capacity for the drugs storage and release, but also exhibit luminescence, which renders it capable of monitoring and evaluating the efficiency and behavior of drug release.[6,8,16] Recently, Zhang et al. reported a facile large-scale synthesis of uniform and well-dispersed MSNs with small particle size (about 100 nm) and tunable pore structure via a templating sol−gel technique.[23] The above MSNs may be considered as a promising candidate for drug carriers. However, the conven-

Received: March 11, 2015
Accepted: May 6, 2015
Published: May 6, 2015

DOI: 10.1021/acsami.5b02146
ACS Appl. Mater. Interfaces 2015, 7, 10905−10914

tional MSNs exhibit no photoluminescence, which may limit their applications in biomedical fields.

Generally, the luminescent MSNs are obtained by the integration of MSNs with luminescent materials, which would confer the resultant nanocomposite abilities of bioimaging and drug delivery. However, the conventional luminescent materials including semiconductor nanoparticles and organic molecules, which exhibit certain drawbacks such as toxicity, photobleaching, and quenching of fluorescence, thereby limiting their applications in biomedical fields.[24,25] In recent years, Lin's group have successfully synthesized a series of multifunctional DDS based on rare earth luminescent materials (such as Fe_3O_4@$nSiO_2$@$mSiO_2$@$NaYF_4$:Yb^{3+},Er^{3+}/Tm^{3+} composites,[26] Gd_2O_3:Eu^{3+}@P(NIPAmco-AAm)@HMS microspheres,[27] NaYF_4:Yb^{3+}/Er^{3+}@hydrogel hybrid microspheres,[28] PAA@$GdVO_4$:Ln^{3+} nanocomposites,[29] $BaGdF_5$-based upconversion nanoparticles,[30] GdOF:Ln@SiO_2 capsules,[31] et al.) and investigated their cytotoxicity, controlled drug release properties as well as therapy functions.[32] However, the accumulation of rare earth nanomaterials in body may cause some adverse bioeffects, such as splenic degeneration, calcium channels blocking, central lobular necrosis of liver, etc.[33,34] So it is highly desirable to develop the novel luminescent MSNs systems with low toxicity, good biocompatibility, and excellent luminescence properties for their biomedical applications. Recently, a series of environmentally friendly and efficient defect-related phosphors (without transition metal or lanthanide ions as activators) have been reported.[6,8,35] These novel defect-related inorganic materials may be applied as multifunctional drug carriers or luminescent materials for biodetection due to their good fluorescent properties, nontoxicity, and excellent biocompatibility.[6,8,35] Therefore, in combining the advantages of biocompatible MSNs and defect-related materials, the design and development of monodisperse defect-related luminescent MSNs may be especially promising for bioapplications, particularly in encapsulation, controlled release, labeling or imaging. Hou et al. reported the porous silica fibers with defect-related luminescence properties as drug carriers, but the biological safety evaluation and therapy effect of the drug carriers were not investigated in detail.[6] Moreover, the large particle size of the porous silica fibers may greatly limit their practical applications.

In this work, we have synthesized monodisperse walnut kernel-like silica nanoparticles with diameters about 100 nm, which exhibit mesoporous structure, small particle size, uniform morphology, good biocompatibility, and high drug loading capacity. In particular, the drug carrier exhibits intense white-blue defect-related luminescence, which can monitor and evaluate the efficiency and behavior of the drug release process. Moreover, the as-synthesized drug delivery system exhibits potent anticancer effect against HeLa, MCF-7, and A549 cells.

EXPERIMENTAL SECTION

Preparation of MSNs and DLMSNs. Monodisperse mesoporous silica nanoparticles (MSNs) and defect-related luminescent mesoporous silica nanoparticles (DLMSNs) were synthesized based on the previous literature with some modifications.[23] In a typical synthesis, 0.9614 g of CTATos and 0.14 mL of $TEAH_3$ were dissolved into 50 mL of deionized water under vigorous magnetic stirring at 80 °C for 1 h to obtain transparent solution. Then, 8 mL of TEOS was quickly introduced into the above solution. Subsequently, the as-obtained mixture was stirred at 80 °C for another 2 h. The resulting precipitates were washed with deionized water and ethanol, and then dried in vacuum at 75 °C to obtain MSNs. Finally, the as-synthesized MSNs were calcinated in air at 230 °C for 2 h to prepare the defect-related luminescent mesoporous silica nanoparticles (DLMSNs).

Materials Characterizations. Scanning electron microscopy (SEM) images were investigated by a field-emission scanning electron microscopy system JSM-7600F (JEOL). Transmission electron microscopy (TEM) images of the nanostructures were obtained by a Tecnai G2 S-Twin transmission electron microscope (FEI). The N_2 adsorption/desorption isotherms, BET surface area, and pore volume was obtained by were obtained on a micromeritics ASAP 2010 M instrument. Particle size was measured with Nanomeasurer 1.2 software from 50 particles in SEM pictures of DLMSNs and MSNs. Zeta potentials were determined using Nano-ZS (Malvern Instruments) in disposable cuvettes. FT-IR spectra were obtained in KBr pellet by PerkinElmer 580B. The loading amount of DOX was determined by thermogravimetry (TG) measurement (Pyris Diamond PerkinElmer). The photoluminescence (PL) spectra were measured on an F-7000 spectrophotometer (Hitachi). All measurements were performed at room temperature.

Cell Culture. Human cervical carcinoma cells (HeLa cells), human breast carcinoma cells (MCF-7 cells), human lung adenocarcinoma cells (A549 cells), and human umbilical vein endothelial cells (HUVE cells, normal cell) were cultured in Dulbecco's modified Eagle's medium, and mouse liver cells (BRL3A cells, normal cell) were cultured in high glucose Dulbecco's modified Eagle's medium, containing with 10% (v/v) fetal bovine serum, 100 U/mL penicillin and 100 μg/mL streptomycin at 37 °C with 5% CO_2.

Cytotoxicity Assay. In vitro cytotoxicity of empty DLMSNs and MSNs was measured by a standard colorimetric 3-(4, 5-dimethylthiazol-2-yl)-2, 5-diphenyl tetrazolium bromide (MTT, Sigma-Aldrich) assay.[36] In brief, HeLa, MCF-7, A549, HUVE, and BRL3A cells were seeded into 96-well plates at 3×10^4/well and cultured overnight at 37 °C in 5% CO_2. Thereafter, the cells were treated with DLMSNs and MSNs (concentration from 1 to 200 μg/mL) for 12 or 24 h. At the end of incubation, 10 μL MTT with concentration of 5 mg/mL was added to each well for another 4 h at 37 °C. Then 100 μL DMSO was added to each well and the plate was examined using the microplate reader (Molecular Devices Versamax, USA) at the absorbance wavelengh of 570 nm. All measurements were performed from three independent experiments.

Biocompatibility. For the detailed procedures of the cellular uptake, Annexin V-FITC/PI staining, lactate dehydrogenase (LDH) release, swelling of lysosome, reactive oxygen species (ROS), and hemolysis assays, see the Supporting Information.

Drug Loading and Release Profile Assay. The amount of DOX loaded into DLMSNs was measured by fluorescence spectrophotometer. In a 1 mL aqueous system, 4 mg of DOX and 2 mg of DLMSNs were mixed and shaken for 24 h at room temperature to obtain the drug carrier system: DLMSNs-DOX. The DOX loading efficiency (LE) on DLMSNs was evaluated by the following formula: $\mathrm{LE}\ (\%) = [m_{(\text{total DOX})} - m_{(\text{DOX in supernatant})}]/[m_{(\text{loaded DOX})} + m_{(\text{carrier})}] \times 100$. The fluorescence of DOX for original and residual in supernatant was both detected at excitation and emission wavelength of 488 and 592 nm, respectively.

The DOX release from DLMSNs-DOX in vitro was measured by a semipermeable dialysis bag diffusion technique. The parallel DLMSNs-DOX were redispersed in 1 mL of acetate buffer (pH 5.0) or 1 mL of PBS (pH 7.4), which was transferred into semipermeable dialysis bags, and then immersed in 10 mL of acetate or PBS buffer at 37 °C with shaking, respectively. At tested time intervals, 10 mL of acetate or PBS buffer were taken out and the amount of released DOX was measured by fluorescence spectroscopy compared to the standard curve, and then an equal volume of fresh acetate buffer or PBS was added to the release system.

Confocal Imaging and Subcellular Localization. The fluorescence of DLMSNs, the cellular drug release, and subcellular localization of DLMSNs-DOX were monitored by confocal laser microscope. The detailed procedures are demonstrated in the Supporting Information.

Anticancer Effect Assay. In vitro cytotoxicity of free DOX and DLMSNs-DOX was measured by MTT assay as described above.

DOI: 10.1021/acsami.5b02146
ACS Appl. Mater. Interfaces 2015, 7, 10905−10914

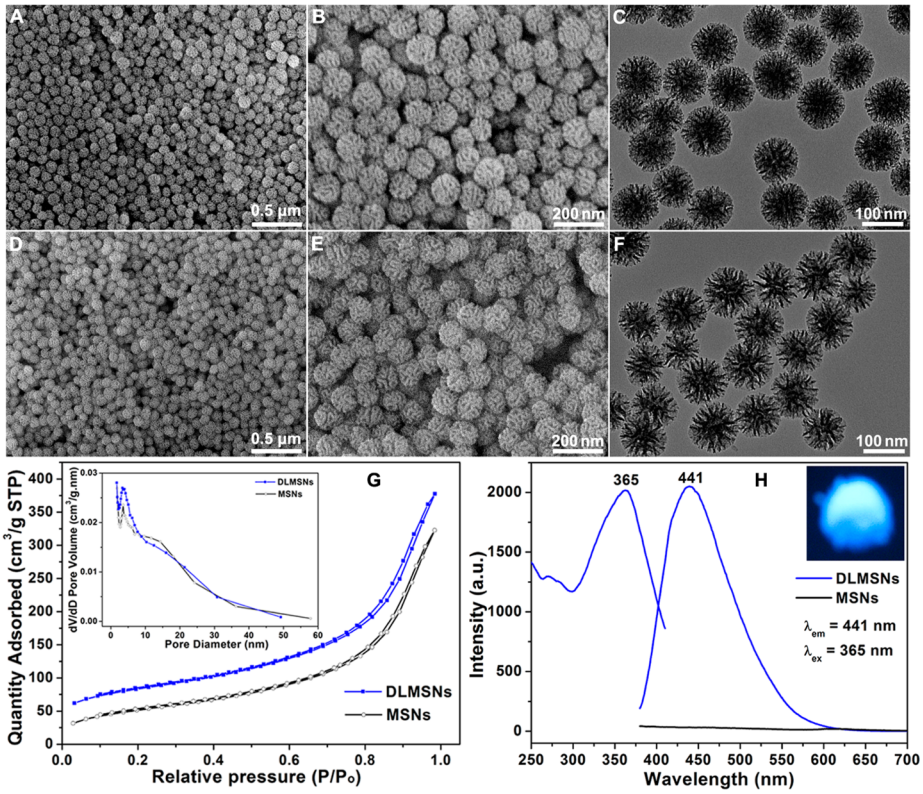

Figure 1. Characterizations of MSNs and DLMSNs. SEM and TEM images of (A−C) MSNs and (D−F) DLMSNs. (G) N_2 sorption isotherms and the corresponding BJH pore size distribution curves (inset) of MSNs and DLMSNs. (H) PL excitation and emission spectra of MSNs and DLMSNs. Inset in H is the corresponding luminescent photograph of DLMSNs under UV excitation (365 nm) in dark.

HeLa, MCF-7, and A549 cells were treated with various concentrations (from 0.04 to 5 μg/mL) of free DOX and DLMSNs-DOX for 12, 24, or 48 h. All measurements were performed from three independent experiments.

Statistical Analysis. Data presented as mean ± standard deviation, which were collected from three separate experiments. Two groups' comparison was determined by two-tail Student's *t* test, and the significant difference was defined as *P* values <0.05 at the 95% confidence interval.

RESULTS

Morphology, Structure, and Luminescence of MSNs and DLMSNs. SEM and TEM images were used to characterize the morphology of the as-obtained MSNs and DLMSNs samples. The calculated size distribution histogram confirmed the size distribution of MSNs and DLMSNs. The low-magnification SEM image of MSNs (Figure 1A) shows that the MSNs sample is composed of high yield monodisperse nanospheres with diameters in the range of 96−144 nm. The particles are nonaggregated and exhibit narrow size distribution (Figure S1a in the Supporting Information). The high-magnification SEM and TEM images (Figure 1B, C) clearly reveal the walnut kernel morphology of MSNs and the existence of uniform mesopores. After an annealing process, the DLMSNs sample mainly consists of uniform and well-dispersed nanospheres with diameters in the range of 79−124 nm (Figure 1D, E and Figure S1b in the Supporting Information), which inherit the morphology of MSNs. However, from the TEM image of DLMSNs (Figure 1F), one can see the more evident mesoporous structure and the increase of center-radial pore sizes, which may induces larger surface area. The result can be confirmed by nitrogen adsorption data (Figure 1G).

The respective N_2 adsorption/desorption isotherms of MSNs and DLMSNs are shown in Figure 1G. It is observed that the two samples reveal typical H1-hysteresis loops and similar N_2 adsorption/desorption isotherms, indicating the typical mesoporous nature. For MSNs, the BET surface area is about 187.4 m^2/g and the pore volume is about 0.50 cm^3/g. After an annealing process, the BET specific surface area and pore volume of DLMSNs increase to 232.9 m^2/g and 0.56 cm^3/g, respectively. Moreover, the narrow peak in the pore size distribution curve increases from 3.5 to 3.7 nm (inset in Figure 1G). Under ultraviolet excitation, MSNs do not exhibit any luminescence (Figure 1H, black line). Figure 1H shows the excitation and emission spectra of DLMSNs (blue line). The excitation spectrum consists of an intense broadband from 200 to 450 nm (centered at 365 nm). The emission spectrum of DLMSNs consists of an intense broadband from 380 to 600 nm (centered at 441 nm) under 365 nm excitation. Inset in Figure 1H shows the luminescent photograph of DLMSNs excited by UV light in the dark (365 nm), which confirms the bright white-blue emission of the DLMSNs sample. Zeta potential measurements were also performed to investigate the surface properties and stability of the nanoparticles. One can see that the zeta potential of MSNs and DLMSNs are −26.1 ± 3.37 and −19.6 ± 4.58 mV in water (Figure S2 in the Supporting Information), indicating that the as-obtained nanoparticles exhibit good stability in water.

Biocompatibility of MSNs and DLMSNs. To evaluate the potential of the nanoparticles as an effective drug carrier, we evaluated the cytotoxicity of MSNs and DLMSNs against

DOI: 10.1021/acsami.5b02146
ACS Appl. Mater. Interfaces 2015, 7, 10905−10914

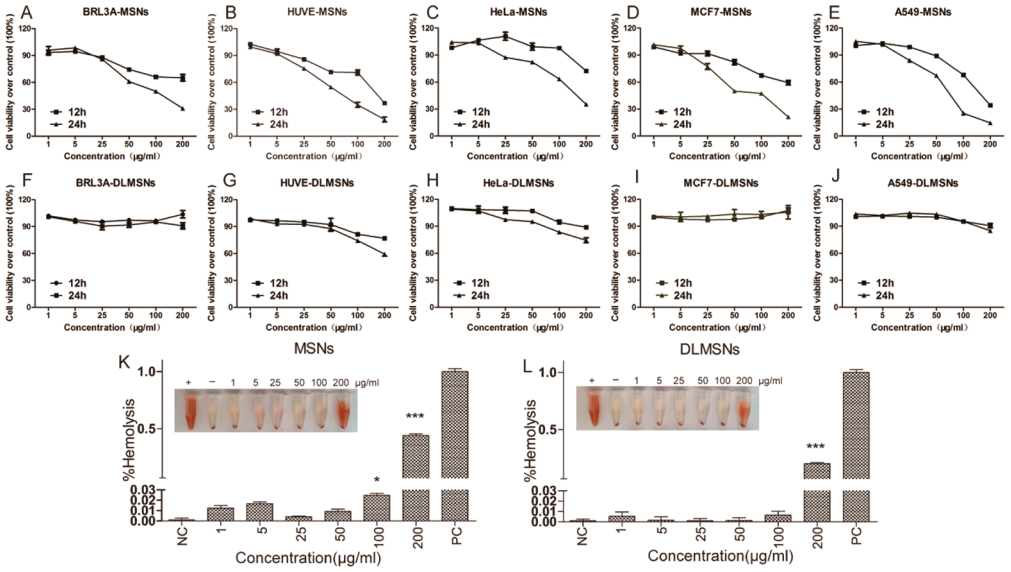

Figure 2. Evaluation of biocompatibility for DLMSNs and MSNs. The cell viability of BRL3A, HUVE, HeLa, MCF7, and A549 cells treated with (A–E) MSNs and (F–J) DLMSNs for 12 and 24 h. Hemolysis phenomena and ratio of red cells incubated with (K) MSNs and (L) DLMSNs.

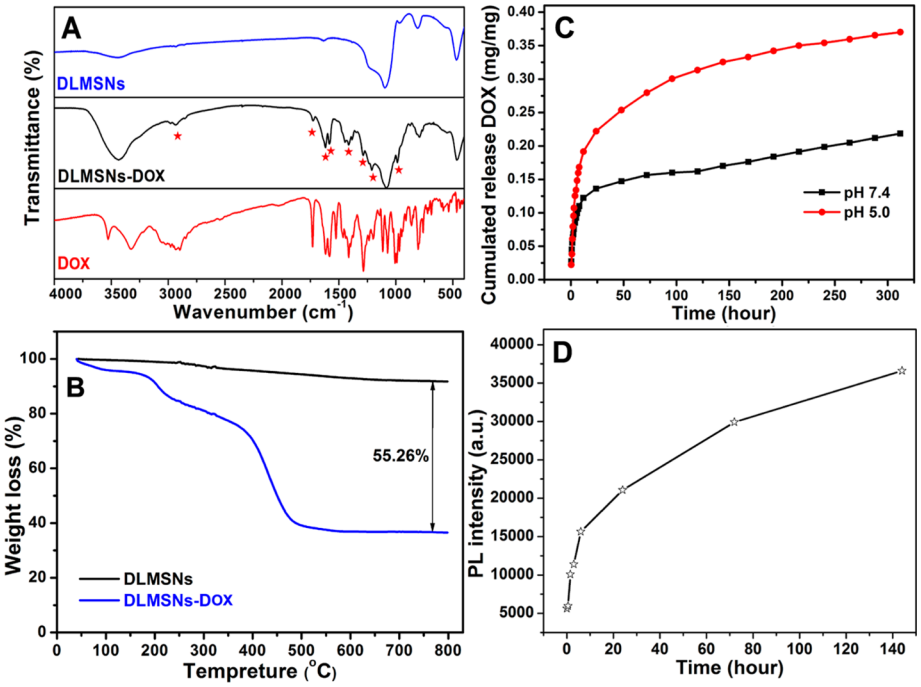

Figure 3. Characterizations and DOX-release profiles of DLMSNs-DOX system. (A) FT-IR spectra of the DLMSNs (blue line), DLMSNs-DOX (black line), and free DOX (red line). (B) TGA curves of DLMSNs and DLMSNs-DOX under a flow of oxygen. (C) DOX-release profiles for DLMSNs-DOX at pH 5.0 and at pH 7.4 at 37 °C. (D) PL emission intensity of DLMSNs-DOX as a function of the cumulatively released DOX.

normal cells (BRL3A and HUVE cells), cancer cells (HeLa, MCF-7 and A549 cells). As shown in Figure 2, those incubated with DLMSNs, BRL3A, MCF-7, and A549 cells show relative high cell viability (>90%) at all tested concentrations for 12 and 24 h (Figure 2F, I, J), HUVE and HeLa cells also display relative high cell viability (>90%) at the concentrations less than 50 μg/mL for 12 and 24 h (Figure 2G, H). However, MSNs sample decreases the cell viability in dose and time manners at all tested concentrations for 12 and 24 h (Figure 2A–E). For example, the viability of HUVE and A549 cells obviously reduce to about 30% after 200 μg/mL treatment for 12 h (Figure 2B, E).

To ascertain whether DLMSNs or MSNs were uptaken by cells, we used a flow cytometer to analyze the uptake of nanoparticles by side scatter signals. Figure S3 in the Supporting Information shows the uptake of DLMSNs and MSNs into BRL3A cells after exposure for 3, 6, 9, 12, and 24 h. The uptake amount of DLMSNs and MSNs exhibits no significant difference at each time point. Annexin V-FITC/PI double staining assay was also performed by flow cytometric analysis to distinguish normal, apoptotic, or necrotic cells. As shown in Figure S4 in the Supporting Information, one can observe that MSNs induces significant increase in the fraction of PI^+ cells in comparison with DLMSNs. Moreover, for MSNs-

DOI: 10.1021/acsami.5b02146
ACS Appl. Mater. Interfaces 2015, 7, 10905–10914

treated BRL3A cells, the percentage of PI^+ cells approximately increases from 22 to 34% by increasing the concentration of MSNs. LDH release test further indicates that MSNs-treated cells exhibit significant LDH increase compared with those of DLMSNs-treated and the control groups (Figure S5 in the Supporting Information), indicating that partial PI(+) cells should be necrosis cells after treatement by MSNs. In addition, the DLMSNs- and MSNs-treated cells were stained by lysotracker green to examine the accumulation effect of the nanoparticles in the lysosome. As shown in Figure S6 in the Supporting Information, the volume of lysosome significantly increases in the MSNs-treated cells, but lysosome in the DLMSNs-treated cells has no significant change compared with that of control cells. As shown in Figure S7 in the Supporting Information, MSNs induce an approximately 1.5-fold increase for ROS level in comparison with that of the untreated group at 24 h, whereas DLMSNs cause about 1.1-fold increase for ROS level.

In addition, DLMSNs at the highest concentration (200 μg/mL) appears to be hemolytic (Figure 2L); however, MSNs show hemolysis at a concentration of 100 μg/mL (Figure 2K). In summary, the results indicate that DLMSNs exhibit better biocompatibility in comparison with MSNs.

DOX Loading and Release Properties. To investigate the controlled release of DLMSNs, we chose DOX as an anticancer drug model to evaluate the loading and release profiles of DLMSNs. The FT-IR spectra of DLMSNs, DLMSNs-DOX, and commercial DOX are shown in Figure 3A. For DLMSNs, the FT-IR spectrum shows characteristic SiO_2 functional groups of Si−O−Si (ν_s: 1098 cm^{-1}, ν_{as}: 814 cm^{-1}), Si−OH (ν_s: 965 cm^{-1}), and Si−O (δ: 469 cm^{-1}).[6] The obvious absorption bands at 1640 and 3436 cm^{-1} are attributed to the O−H vibration and −OH group from H_2O, indicating that a large amount of −OH groups and H_2O are present in DLMSNs, which are important for binding hydrophilic DOX drug molecules. For DLMSNs-DOX, the FT-IR spectrum includes all the absorption bands of bare DLMSNs and DOX, and no new absorption band can be detected, indicating that the DOX has been successfully absorbed on DLMSNs. The loading capacity of DOX into the DLMSNs is about 1400 mg/g at a similar DOX concentration, which means that the loading efficiency is 58.33%. The quantitative amount of DOX adsorbed into DLMSNs was also monitored by thermogravimetric (TG) analysis (Figure 3B). One can see that the respective DOX loading degree of DLMSNs is determined to be 55.26 wt %, which agrees well with the calculated value.

In vitro release profiles of DOX from DLMSNs were examined in PBS buffer at pH 7.4 and pH 5.0. From Figure 3C, one can observe that the DLMSNs-DOX system shows an initial burst release within 12 h, followed by a slow sustained release of DOX molecules. The drug release process for the DLMSNs-DOX system can sustain for more than 300 h. The initial release may be assigned to the weak adsorption of the DOX on the outer surface of DLMSNs, and the slow sustained release of DOX can be assigned to the strong interaction between DLMSNs and DOX.[6,8,16] Moreover, the drug release rate of DLMSNs at pH 5.0 is faster than that of at pH 7.4, which indicates that DLMSNs can improve the drug release efficiency in acidic medium.

The emission intensity of DLMSNs-DOX system as a function of the cumulative amount of released DOX is shown in Figure 3D. One can observe that the emission intensity of DLMSNs-DOX increases with prolonged release time, which means that the emission intensity increases with the cumulative release of DOX.

Imaging of DLMSNs-DOX. The fluorescence of empty DLMSNs, free DOX, and DOX-DLMSNs in HeLa cells was tested by confocal laser scanning microscopy under the excitation wavelength of 405 nm for DLMSNs and 488 nm for DOX. As shown in Figure 4, when HeLa cells were

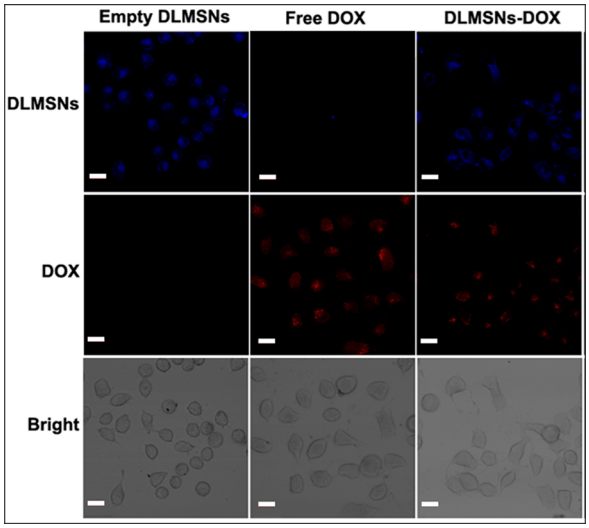

Figure 4. Confocal images of intracellular internalization of empty DLMSNs, free DOX, and DLMSNs-DOX (5 mg/mL) for 9 h at 37 °C. Scale bar is 20 μm.

incubated by empty DLMSNs, only the fluorescence of DLMSNs appeared. When HeLa cells were incubated with free DOX, only the fluorescence of DOX could be detected. When HeLa cells were incubated with DLMSNs-DOX, the fluorescence of both DLMSNs and DOX was observed. In addition, we also investigated the changes of luminescence intensity of released DOX in cells at the condition that 5 ug/mL DOX loaded DLMSNs for 1, 3, 6, 9, 12, and 24 h. As shown in Figure 5, the fluorescence intensity of DOX increases gradually with the increase of release time, which agrees well with in vitro drug release data in Figure 3D. Moreover, it should be pointed out that the fluorescence intensity of DLMSNs also increases with the increase in release time.

To investigate the intracellular localization of DOX released from the DLMSNs-DOX, we labeled HeLa cells with a specialized dye for lysosome labeling (LysoTracker Green DND-26). One can see that free DOX was mostly localized in the cytoplasm after 9 h incubation. By contrast, the DLMSNs-DOX was primarily distributed in lysosome (Figure 6).

Anticancer Effect. To evaluate the anticancer effect of DLMSNs-DOX, we investigated in vitro cytotoxicity of free DOX and DLMSNs-DOX against HeLa, MCF-7, and A549 cells. Three kinds of cells were incubated with free DOX and DLMSNs-DOX, and the concentration of DOX was used as equivalent concentration in all biological experiments. It could be seen from Figure 7 that DLMSNs-DOX exhibited a potent anticancer effect against three kinds of cancer cells in a dose-dependent manner for 12, 24, and 48 h, with results comparable to free DOX.

DOI: 10.1021/acsami.5b02146
ACS Appl. Mater. Interfaces 2015, 7, 10905−10914

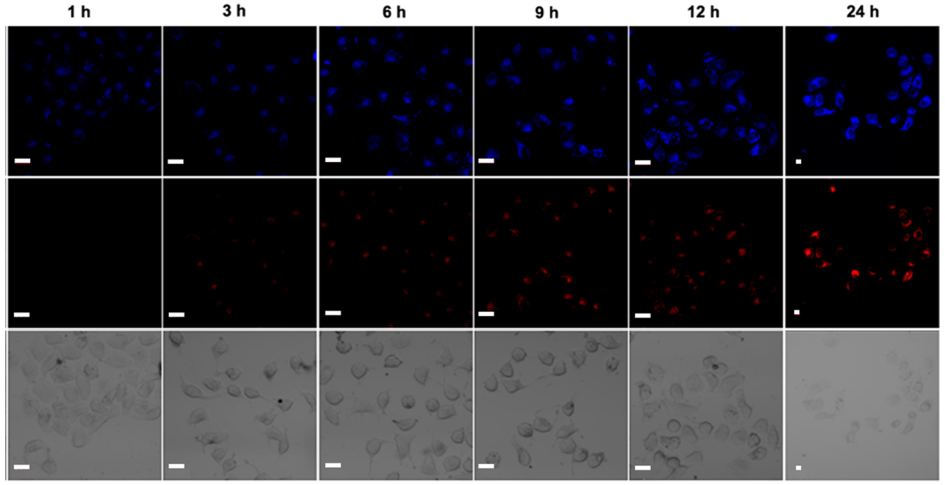

Figure 5. Confocal images of DLMSNs-DOX (5 mg/mL DOX) in HeLa cells for 1, 3, 6, 9, 12, and 24 h at 37 °C. The DLMSNs or DOX fluorescence is defined as blue or red, respectively. Scale bar is 20 μm.

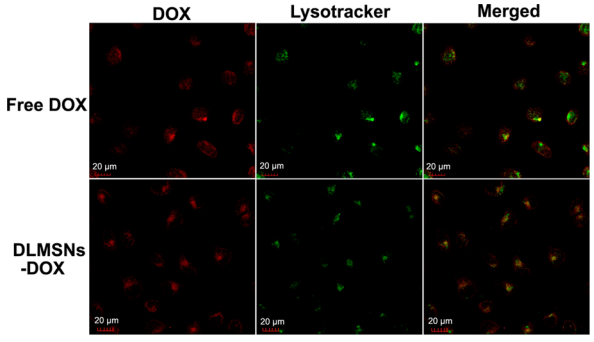

Figure 6. Confocal images of intracellular distribution of DLMSNs-DOX and free DOX in HeLa cells.

DISCUSSION

An ideal DDS generally possesses some properties, including good biocompatibility, appropriate particle size and narrow size distribution, targeting ability, and sustained and controlled drug release manner.[8,9] As an important class of biomaterials, MSNs have been studied as drug carriers because of their tunable particle size, high loading capacity, and good biocompatibility.[6,25] To date, there have been few reports on the facile synthesis of the hierarchical MSNs with smaller particle size and their applications in the biomedical field. Recently, Zhang et al. have successfully synthesized monodisperse MSNs with tunable pore structure and smaller particle size by a templating sol−gel route.[23] In this paper, in accordance with established techniques, we have (with some modifications) successfully synthesized the high yield monodisperse walnut kernel-like MSNs with diameters of about 100 nm (Figure 1). However, the biocompatibility test reveals that the as-obtained MSNs exhibits cytotoxicity to some extent and a relatively poor biocompatibility (Figure 2), which may seriously undermine their biomedical application. After an annealing process, the as-synthesized DLMSNs sample, which inherits the well-defined morphology and good dispersion of MSNs, exhibits lower cytotoxicity and better biocompatibility (Figure 1 and 2). In addition, the BET specific surface area and pore volume and size increase during the annealing process (Figure 1G), which is advantageous and favorable for the high drug loading capacity of drug carriers. Furthermore, during the annealing process, some carbon defects were introduced into the MSNs host, resulting in a bright white-blue emission in the rage of 380−600 nm (centered at 441 nm) (Figure 1H). In the synthesis process, TEOS was hydrolyzed to form −Si−O−Si− networks and CH_3−CH_2−O−Si− groups. Most organic compounds were removed by washing with H_2O and ethanol, and the residual organic additives and ethyl groups still existed in SiO_2 networks. When heated, the residual organic components may decompose and the cleavage occurred in the C−O bonds to create carbon substitutional defects in the networks (−Si−O−C−O−Si−), which was assumed to be the luminescent species in the silica lattice.[37] Under the UV excitation, the as-formed −Si−O−C−O−Si− cleaved into −Si−O−C• and •O−Si−, which included an electron localized in 2p orbital of the C−O bonds. These defect centers would induce luminescence via strong electron-photon coupling.[37−39] Thus, the defect-related luminescent carrier may confer a possibility to monitor and track the carrier fate, which is of considerable significance for systematically studying the metabolic pathways of inorganic drug carriers.

In the drug-loaded carrier system, great emphasis has been put on the drug release and the subsequent cytology effect. In particular, more attention should be paid for the biocompatibility of carrier itself. It is well-known that efficiency and safety of nanoparticles is crucial for drug carriers. In terms of cytotoxicity, many factors may affect the potential toxicity of nanoparticles including the particle size, morphology, surface charge, chemical compositions, aggregation tendency, and surface functionalization. These factors would also influence the target cellular compartments when the nanoparticles were uptaken by cells, which may induce significant toxic effects during the process.[40,41]

In our work, DLMSNs and MSNs are taken almost equally by BRL3A cells at each time point (Figure S3 in the Supporting Information), but the death rate of MSNs-treated BRL3A cells is higher than that of DLMSNs-treated cells as revealed by PI binding (Figure S4 in the Supporting Information). As we know, necrotic cells generally undergo damage of organelle and plasma membrane and release intracellular components such as LDH. The concentration of released LDH from cells to medium can be used to quantify the necrosis. It can also be seen that the concentration of released LDH in MSN-treated cells is much higher than those of DLMSNs-treated and control

DOI: 10.1021/acsami.5b02146
ACS Appl. Mater. Interfaces 2015, 7, 10905−10914

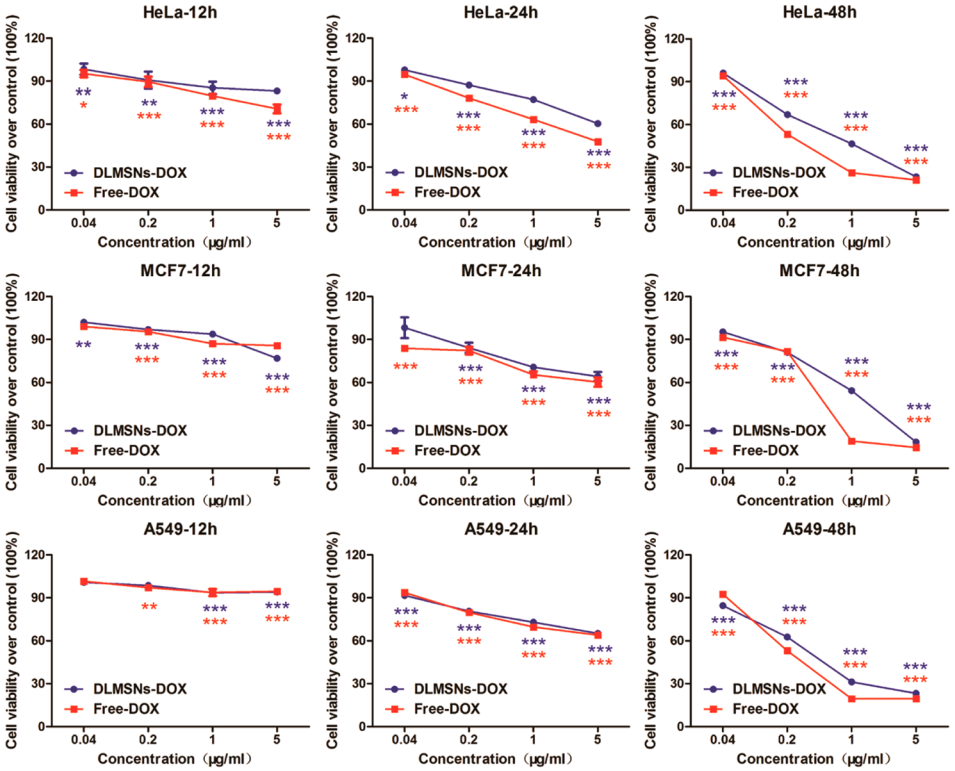

Figure 7. Anticancer effect of DLMSNs-DOX and free DOX. In vitro viability of HeLa, MCF-7, and A549 cells incubated with DLMSNs-DOX and free DOX for 12, 24, and 48 h. Cell viability between two groups were analyzed with concentration of DLMSNs-DOX and free DOX under different treatment time (*P < 0.05, **P < 0.01, ***P < 0.001).

groups (Figure S5 in the Supporting Information). Lysosomes as hydrolase-rich organelles are acidic and play a crucial role in intracellular protein recycling, which is closely related to cell death process.[42,43] Generally, the destabilization of lysosomal proteins induces lysosomal membrane permeabilization (LMP). In this case, the accumulation of MSNs into lysosome may cause permeabilization of lysosomal membranes. MSNs-induced permeabilization causes an influx of water and leads to lysosomal swelling (Figure S6 in the Supporting Information). The swelling lysosomes are apt to break down and cause cytosolic acidification, followed with the degradation of intracellular compartments and resulting in necrosis.[43] It can be concluded that the cell toxicity induced by MSNs and DLMSNs may have no relationship with their uptake, but there is a significant relationship with lysosome permibility.

On the other hand, oxidative stress has been considered the common way for nanomaterial-induced toxicity.[44] ROS, which may cause lysosomal membrane permeabilization, is essential in signal transduction for cell growth and proliferation. High level of ROS generally induces various dysfunctions of cells including the damage of membrane, DNA, and protein, apoptosis, or necrosis.[45] In our study, the ROS level of MSNs-treated cells are much higher than those of DLMSNs-treated and the control groups (Figure S7 in the Supporting Information). The result reveals that the MSNs-induced cell death through necrosis involving early lysosomal destabilization and intracellular ROS increase, which further indicates that DLMSNs exhibit better biocompatibility than that of MSNs and may be more suitable for drug delivery.

As an efficient drug carrier, the high drug-loading capacity is necessary. The loading capacity of the as-synthesized DLMSNs is about 1400 mg/g DOX with loading efficiency of 58.33%, which exhibits the high drug-loading capacity. The result has also been confirmed by TG analysis (Figure 3B). From DOX release profile in vitro, the DLMSNs-DOX system shows an initial burst release within 12 h, followed by the slow sustained release process (Figure 3C). During the carcinoma treatment, the initial burst release is favorable in order to reach a sufficient dosage of drugs, which can effectively prevent tumor growth. On the other hand, the sustainable release is desirable to inhibit the proliferation of the survival cancer cells.[19] The overall release process of the DLMSNs-DOX can sustain for more than 300 h. Such prolonged and gradual release behavior is preferable for the enhanced efficiency of tumor therapy, because continually sustained DOX release from carrier can effectively prevent tumor growth in long-term treatment.[3] The cumulative drug release of DOX from DLMSNs carrier in PBS (pH 7.4) exhibits slower release than in acetate buffer (pH 5.0) (Figure 3C). This is because the protons can easily penetrate the mesopores in acidic buffer solution to protonate the amino group of DOX, thus accelerating the drug release.[46] The pH-sensitive release behavior is preferable for tumor therapy. In this case, most of the anticancer drug can remain encapsulated in DLMSNs during circulation, but the drug release can be triggered when the DLMSNs-DOX reaches the acidic tumor tissues. The similar pH-responsive release properties were also reported for other nanocarriers in previous literatures.[47,48]

Fluorescence is one of the attractive detection methods in proteomics, genomics, and cell biology. In particular, the fluorescent nanoparticles has been widely utilized as biolabeling, which leads to major advances in biomedical imaging.[49,50] In the drug delivery field, the luminescent drug carriers can monitor the drug release behavior.[6,8,16] Because of the uniform morphology, mesoporous structure, large surface areas, good

DOI: 10.1021/acsami.5b02146
ACS Appl. Mater. Interfaces 2015, 7, 10905−10914

biocompatibility as well as excellent luminescence properties, the as-synthesized DLMSNs may be potentially applied as a promising detectable drug carrier in drug delivery field. The PL emission intensity of DLMSNs-DOX system as a function of the cumulative amount of released DOX was also investigated (Figure 3D). With the increase in release time, the PL intensity of DLMSNs in DLMSNs-DOX system gradually increases with the cumulative released DOX. The reason may be that the DOX molecules harbor the ability to quench some luminescent centers of DLMSNs, thus decreasing the luminescence intensity of drug carrier. By increasing the release time, the quenched luminescent centers of DLMSNs can recover accompanied by the release of DOX, which result in the enhancement of the PL emission intensity. On the basis of the relationship between the fluorescence intensity and drug release extent, the as-synthesized drug carrier DLMSNs can be potentially applied as a luminescent probe for tracking the drug release process. The similar result was also verified by the confocal laser scanning images of DLMSNs-DOX releasing in HeLa cells (Figure 5). It can be observed that the brightness of DOX and DLMSNs increase gradually with prolonged release time (Figure 5).

To further evaluate the efficiency of the drug-loading system for tumor therapy in vitro, we first investigated the intracellular localization of DLMSNs-DOX system. After incubation with HeLa cells for 9 h, most free DOX was localized in the cytoplasm, whereas the DLMSNs-DOX was primarily distributed in the lysosome (Figure 6). Thus, the DOX can efficiently release from the DLMSNs-DOX system which was mainly distributed in lysosome due to the acidic environment of lysosome (pH 5.0).[48,51,52] The released DOX from DLMSNs-DOX increased in the cytoplasm with elapsed time (Figure 5). The above results suggest that the DLMSNs-DOX may induce a continual release of DOX and ensure a sustained and sufficient DOX dosage to continually kill tumor cells.[52] In vitro cytotoxicity of free DOX and DLMSNs-DOX against HeLa, MCF-7,and A549 cells was also studied. The results indicated that DLMSNs-DOX exhibited a potent anticancer effect against three kinds of cancer cells in a dose-dependent manner for 12, 24, and 48 h (Figure 7), with results comparable to those of free DOX.

CONCLUSIONS

Monodisperse DLMSNs with diameters about 100 nm have been fabricated by a templating sol−gel route followed by an annealing treatment. The as-obtained DLMSNs drug carrier exhibits well-defined morphology, excellent biocompatibility, high drug loading capacity, bright luminescence as well as high drug loading capacity. The emission intensity and confocal laser scanning images indicate that the PL luminescence of DLMSNs increases gradually with the sustained release of DOX in the DLMSNs-DOX system. The as-synthesized DLMSNs material may be potentially applied as a luminescent carrier in detecting the drug release behavior. Moreover, the DDS exhibits a potent anticancer effect against three kinds of cancer cells. Because of the uniform morphology, mesoporous structure, large surface areas and pore volume, good biocompatibility, as well as excellent luminescence properties, the as-synthesized DLMSNs may well function as a promising detectable drug carrier in the drug-delivery field.

ASSOCIATED CONTENT

Supporting Information

Description of biocompatibility assay, the fluorescence of DLMSNs, the cellular drug release and subcellular localization of DLMSNs-DOX details. The Supporting Information is available free of charge on the ACS Publications website at DOI: 10.1021/acsami.5b02146.

AUTHOR INFORMATION

Corresponding Authors

*E-mail: guangjia2001@163.com.
*E-mail: liangxj@nanoctr.cn.
*E-mail: jczhang6970@163.com.

Author Contributions

†K.G. and C.Z. contributed equally to the manuscript.

Notes

The authors declare no competing financial interest.

ACKNOWLEDGMENTS

This research was supported by the National Natural Science Foundations of China (31470961, 21001038, 21301046, 51302062), the Research Fund for the Doctoral Program of Higher Education of China (20111301110004, 20131301120004), Hebei Province "Hundred Talents Program" (BR2-202), Hebei Province "Three Three Three Talents Program" (A201401002), Key Basic Research Special Foundation of Science Technology Ministry of Hebei Province (14961302D), the China Postdoctoral Science Foundation Funded Project (2013M530119, 2014T70226), the Outstanding Youth Fund Project of Hebei Education Department (Y2012007), Training Program for Innovative Research Team and Leading Talent in Hebei Province University (LJRC024), the Research Fund of State Key Laboratory of Rare Earth Resource Utilization (RERU2015025), and SRF for ROCS, SEM.

REFERENCES

(1) Peng, F.; Su, Y.; Wei, X.; Lu, Y.; Zhou, Y.; Zhong, Y.; Lee, S. T.; He, Y. Silicon-Nanowire-Based Nanocarriers with Ultrahigh Drug-Loading Capacity for *in vitro* and *in vivo* Cancer Therapy. *Angew. Chem., Int. Ed.* **2013**, *52*, 1457−1461.

(2) Zhao, Y.; Trewyn, B. G.; Slowing, I. I.; Lin, V. S. Mesoporous Silica Nanoparticle-Based Double Drug Delivery System for Glucose-Responsive Controlled Release of Insulin and Cyclic AMP. *J. Am. Chem. Soc.* **2009**, *131*, 8398−8400.

(3) Rim, H. P.; Min, K. H.; Lee, H. J.; Jeong, S. Y.; Lee, S. C. pH-Tunable Calcium Phosphate Covered Mesoporous Silica Nanocontainers for Intracellular Controlled Release of Guest Drugs. *Angew. Chem., Int. Ed.* **2011**, *50*, 8853−8857.

(4) Shi, J.; Xu, Y.; Xu, X.; Zhu, X.; Pridgen, E.; Wu, J.; Votruba, A. R.; Swami, A.; Zetter, B. R.; Farokhzad, O. C. Hybrid Lipid-Polymer Nanoparticles for Sustained siRNA Delivery and Gene Silencing. *Nanomedicine* **2014**, *10*, 897−900.

(5) Zhou, W.; Gao, P.; Shao, L.; Caruntu, D.; Yu, M.; Chen, J.; O'Connor, C. J. Drug-Loaded, Magnetic, Hollow Silica Nanocomposites for Nanomedicine. *Nanomedicine* **2005**, *1*, 233−237.

(6) Hou, Z.; Zhang, C.; Li, C.; Xu, Z.; Cheng, Z.; Li, G.; Wang, W.; Peng, C.; Lin, J. Luminescent Porous Silica Fibers as Drug Carriers. *Chem.—Eur. J.* **2010**, *16*, 14513−14519.

(7) Lopez, T.; Ortiz, E.; Alexander-Katz, R.; Basaldella, E.; Bokhimi, X. Cortisol Controlled Release by Mesoporous Silica. *Nanomedicine* **2009**, *5*, 170−177.

(8) Zhang, C.; Li, C.; Huang, S.; Hou, Z.; Cheng, Z.; Yang, P.; Peng, C.; Lin, J. Self-Activated Luminescent and Mesoporous Strontium

DOI: 10.1021/acsami.5b02146
ACS Appl. Mater. Interfaces 2015, 7, 10905−10914

Hydroxyapatite Nanorods for Drug Delivery. *Biomaterials* **2010**, *31*, 3374−3383.
(9) Vivero-Escoto, J. L.; Slowing, I. I.; Wu, C.; Lin, V. S. Photoinduced Intracellular Controlled Release Drug Delivery in Human Cells by Gold-Capped Mesoporous Silica Nanosphere. *J. Am. Chem. Soc.* **2009**, *131*, 3462−3463.
(10) Slowing, I. I.; Trewyn, B. G.; Giri, S.; Lin, V. S. Mesoporous Silica Nanoparticles for Drug Delivery and Biosensing Applications. *Adv. Funct. Mater.* **2007**, *17*, 1225−1236.
(11) Zhang, J.; Yuan, Z. F.; Wang, Y.; Chen, W. H.; Luo, G. F.; Cheng, S. X.; Zhuo, R. X.; Zhang, X. Z. Multifunctional Envelope-Type Mesoporous Silica Nanoparticles for Tumor-Triggered Targeting Drug Delivery. *J. Am. Chem. Soc.* **2013**, *135*, 5068−5073.
(12) Zhang, Q.; Neoh, K. G.; Xu, L.; Lu, S.; Kang, E. T.; Mahendran, R.; Chiong, E. Functionalized Mesoporous Silica Nanoparticles with Mucoadhesive and Sustained Drug Release Properties for Potential Bladder Cancer Therapy. *Langmuir* **2014**, *30*, 6151−6161.
(13) Jana, A.; Nguyen, K. T.; Li, X.; Zhu, P.; Tan, N. S.; Agren, H.; Zhao, Y. Perylene-Derived Single-Component Organic Nanoparticles with Tunable Emission: Efficient Anticancer Drug Carriers with Real-Time Monitoring of Drug Release. *ACS Nano* **2014**, *8*, 5939−5952.
(14) Wu, X.; Wu, M.; Zhao, J. X. Recent Development of Silica Nanoparticles as Delivery Vectors for Cancer Imaging and Therapy. *Nanomedicine* **2014**, *10*, 297−312.
(15) Yang, P.; Gai, S.; Lin, J. Functionalized Mesoporous Silica Materials for Controlled Drug Delivery. *Chem. Soc. Rev.* **2012**, *41*, 3679−3698.
(16) Zhang, X.; Yang, P.; Dai, Y.; Ma, P.; Li, X.; Cheng, Z.; Hou, Z.; Kang, X.; Li, C.; Lin, J. Multifunctional Up-Converting Nanocomposites with Smart Polymer Brushes Gated Mesopores for Cell Imaging and Thermo/pH Dual-Responsive Drug Controlled Release. *Adv. Funct. Mater.* **2013**, *23*, 4067−4078.
(17) He, Y.; Zhong, Y.; Peng, F.; Wei, X.; Su, Y.; Lu, Y.; Su, S.; Gu, W.; Liao, L.; Lee, S. T. One-Pot Microwave Synthesis of Water-Dispersible, Ultraphoto- and pH-Stable, and Highly Fluorescent Silicon Quantum Dots. *J. Am. Chem. Soc.* **2011**, *133*, 14192−14195.
(18) Bhakta, G.; Sharma, R. K.; Gupta, N.; Cool, S.; Nurcombe, V.; Maitra, A. Multifunctional Silica Nanoparticles with Potentials of Imaging and Gene Delivery. *Nanomedicine* **2011**, *7*, 472−479.
(19) Du, X.; Shi, B.; Liang, J.; Bi, J.; Dai, S.; Qiao, S. Z. Developing Functionalized Dendrimer-Like Silica Nanoparticles with Hierarchical Pores as Advanced Delivery Nanocarriers. *Adv. Mater.* **2013**, *25*, 5981−5985.
(20) Li, Y.; Cheng, Q.; Jiang, Q.; Huang, Y.; Liu, H.; Zhao, Y.; Cao, W.; Ma, G.; Dai, F.; Liang, X.; Liang, Z.; Zhang, X. Enhanced Endosomal/Lysosomal Escape by Distearoyl Phosphoethanolamine-Polycarboxybetaine Lipid for Systemic Delivery of siRNA. *J. Controlled Release* **2014**, *176*, 104−114.
(21) Shi, D. L.; Lian, J.; Wang, W.; Liu, G. K.; He, P.; Dong, Z. Y.; Wang, L. M.; Ewing, R. C. Luminescent Carbon Nanotubes by Surface Functionalization. *Adv. Mater.* **2006**, *18*, 189−193.
(22) Lin, Y. S.; Wu, S. H.; Hung, Y.; Chou, Y. H.; Chang, C.; Lin, M. L.; Tsai, C. P.; Mou, C. Y. Multifunctional Composite Nanoparticles: Magnetic, Luminescent, and Mesoporous. *Chem. Mater.* **2006**, *18*, 5170−5172.
(23) Zhang, K.; Xu, L. L.; Jiang, J. G.; Calin, N.; Lam, K. F.; Zhang, S. J.; Wu, H. H.; Wu, G. D.; Albela, B.; Bonneviot, L.; Wu, P. Facile Large-Scale Synthesis of Monodisperse Mesoporous Silica Nanospheres with Tunable Pore Structure. *J. Am. Chem. Soc.* **2013**, *135*, 2427−2430.
(24) Yong, K. T.; Ding, H.; Roy, I.; Law, W. C.; Bergey, E. J.; Maitra, A.; Prasad, P. N. Imaging Pancreatic Cancer Using Bioconjugated InP Quantum Dots. *ACS Nano* **2009**, *3*, 502−510.
(25) Yang, P. P.; Quan, Z. W.; Hou, Z. Y.; Li, C. X.; Kang, X. J.; Cheng, Z. Y.; Lin, J. A Magnetic, Luminescent and Mesoporous Core−Shell Structured Composite Material as Drug Carrier. *Biomaterials* **2009**, *30*, 4786−4795.
(26) Gai, S.; Yang, P.; Li, C.; Wang, W.; Dai, Y.; Niu, N.; Lin, J. Synthesis of Magnetic, Up-Conversion Luminescent, and Mesoporous Core−Shell-Structured Nanocomposites as Drug Carriers. *Adv. Funct. Mater.* **2010**, *20*, 1166−1172.
(27) Kang, X.; Cheng, Z.; Yang, D.; Ma, P.; Shang, M.; Peng, C.; Dai, Y.; Lin, J. Design and Synthesis of Multifunctional Drug Carriers Based on Luminescent Rattle-Type Mesoporous Silica Microspheres with a Thermosensitive Hydrogel as a Controlled Switch. *Adv. Funct. Mater.* **2012**, *22*, 1470−1481.
(28) Dai, Y.; Ma, P.; Cheng, Z.; Kang, X.; Zhang, X.; Hou, Z.; Li, C.; Yang, D.; Zhai, X.; Lin, J. Up-Conversion Cell Imaging and pH-Induced Thermally Controlled Drug Release from $NaYF_4$:Yb^{3+}/Er^{3+}@hydrogel Core-Shell Hybrid Microspheres. *ACS Nano* **2012**, *6*, 3327−3338.
(29) Kang, X.; Yang, D.; Dai, Y.; Shang, M.; Cheng, Z.; Zhang, X.; Lian, H.; Ma, P.; Lin, J. Poly(acrylic acid) Modified Lanthanide-Doped $GdVO_4$ Hollow Spheres for Up-Conversion Cell Imaging, MRI and pH-Dependent Drug Release. *Nanoscale* **2013**, *5*, 253−261.
(30) Yang, D.; Dai, Y.; Liu, J.; Hou, Y.; Chen, Y.; Li, C.; Ma, P.; Lin, J. Ultra-Small $BaGdF_5$-Based Upconversion Nanoparticles as Drug Carriers and Multimodal Imaging Probes. *Biomaterials* **2014**, *35*, 2011−2023.
(31) Lv, R.; Yang, P.; He, F.; Gai, S.; Li, C.; Dai, Y.; Yang, G.; Lin, J. A Yolk-like Multifunctional Platform for Multimodal Imaging and Synergistic Therapy Triggered by a Single Near-Infrared Light. *ACS Nano* **2015**, *9*, 1630−1647.
(32) Gai, S.; Li, C.; Yang, P.; Lin, J. Recent Progress in Rare Earth Micro/Nanocrystals: Soft Chemical Synthesis, Luminescent Properties, and Biomedical Applications. *Chem. Rev.* **2014**, *114*, 2343−2389.
(33) Idée, J. M.; Port, M.; Raynal, I.; Schaefer, M.; Le Greneur, S.; Corot, C. Clinical and Biological Consequences of Transmetallation Induced by Contrast Agents for Magnetic Resonance Imaging: a Review. *Fundam. Clin. Pharmacol.* **2006**, *20*, 563−576.
(34) Liu, H.; Zhang, C.; Tan, Y.; Wang, J.; Wang, K.; Zhao, Y.; Jia, G.; Hou, Y.; Wang, S.; Zhang, J. Biodistribution and Toxicity Assessment of Europium-Doped Gd_2O_3 Nanotubes in Mice after Intraperitoneal Injection. *J. Nanopart. Res.* **2014**, *16*, 2303−2308.
(35) Zhang, C.; Lin, J. Defect-Related Luminescent Materials: Synthesis, Emission Properties and Applications. *Chem. Soc. Rev.* **2012**, *41*, 7938−7961.
(36) Zhang, D. W.; Yi, C. Q.; Zhang, J. C.; Chen, Y.; Yao, X. S.; Yang, M. S. The Effects of Carbon Nanotubes on the Proliferation and Differentiation of Primary Osteoblasts. *Nanotechnology* **2007**, *18*, 475102.
(37) Green, W. H.; Le, K. P.; Grey, J.; Au, T. T.; Sailor, M. J. White Phosphors from a Silicate-Carboxylate Sol-Gel Precursor That Lack Metal Activator Ions. *Science* **1997**, *276*, 1826−1828.
(38) Jakob, A. M.; Schmedake, T. A. A Novel Approach to Monodisperse, Luminescent Silica Spheres. *Chem. Mater.* **2006**, *18*, 3173−3175.
(39) Zhang, C.; Li, C.; Yang, J.; Cheng, Z.; Hou, Z.; Fan, Y.; Lin, J. Tunable Luminescence in Monodisperse Zirconia Spheres. *Langmuir* **2009**, *25*, 7078−7083.
(40) Shahbazi, M. A.; Almeida, P. V.; Mäkilä, E. M.; Kaasalainen, M. H.; Salonen, J. J.; Hirvonen, J. T.; Santos, H. A. Augmented Cellular Trafficking and Endosomal Escape of Porous Silicon Nanoparticles via Zwitterionic Bilayer Polymer Surface Engineering. *Biomaterials* **2014**, *35*, 7488−7500.
(41) Lewinski, N.; Colvin, V.; Drezek, R. Cytotoxicity of Nanoparticles. *Small* **2008**, *4*, 26−49.
(42) Johansson, A. C.; Appelqvist, H.; Nilsson, C.; Kagedal, K.; Roberg, K.; Ollinger, K. Regulation of Apoptosis-Associated Lysosomal Membrane Permeabilization. *Apoptosis* **2010**, *15*, 527−540.
(43) Boya, P.; Kroemer, G. Lysosomal Membrane Permeabilization in Cell Death. *Oncogene* **2008**, *27*, 6434−6451.
(44) Foldbjerg, R.; Dang, D. A.; Autrup, H. Cytotoxicity and Genotoxicity of Silver Nanoparticles in the Human Lung Cancer Cell Line, A549. *Arch. Toxicol.* **2011**, *85*, 743−750.
(45) Wang, L.; Liu, Y.; Li, W.; Jiang, X.; Ji, Y.; Wu, X.; Xu, L.; Qiu, Y.; Zhao, K.; Wei, T.; Li, Y.; Zhao, Y.; Chen, C. Selective Targeting of

DOI: 10.1021/acsami.5b02146
ACS Appl. Mater. Interfaces 2015, 7, 10905−10914

Gold Nanorods at the Mitochondria of Cancer Cells: Implications for Cancer Therapy. *Nano Lett.* **2010**, *11*, 772−780.
(46) Hu, X.; Hao, X.; Wu, Y.; Zhang, J.; Zhang, X.; Wang, P. C.; Zou, G.; Liang, X. J. Multifunctional Hybrid Silica Nanoparticles for Controlled Doxorubicin Loading and Release with Thermal and pH Dual Response. *J. Mater. Chem. B* **2013**, *1*, 1109−1118.
(47) Liu, Z.; Sun, X.; Nakayama-Ratchford, N.; Dai, H. Supramolecular Chemistry on Water-Soluble Carbon Nanotubes for Drug Loading and Delivery. *ACS Nano* **2007**, *1*, 50−56.
(48) Zhang, L.; Lu, Z.; Zhao, Q.; Huang, J.; Shen, H.; Zhang, Z. Enhanced Chemotherapy Efficacy by Sequential Delivery of Sirna and Anticancer Drugs Using PEI-Grafted Graphene Oxide. *Small* **2011**, *7*, 460−464.
(49) Yang, Y.; Shao, Q.; Deng, R.; Wang, C.; Teng, X.; Cheng, K.; Cheng, Z.; Huang, L.; Liu, Z.; Liu, X.; Xing, B. *In vitro* and *in vivo* Uncaging and Bioluminescence Imaging by Using Photocaged Upconversion Nanoparticles. *Angew. Chem., Int. Ed.* **2012**, *51*, 3125−3129.
(50) Zhou, J.; Sun, Y.; Du, X.; Xiong, L.; Hu, H.; Li, F. Dual-Modality *in vivo* Imaging Using Rare-Earth Nanocrystals with Near-Infrared to Near-Infrared (NIR-to-NIR) Upconversion Luminescence and Magnetic Resonance Properties. *Biomaterials* **2010**, *31*, 3287−3295.
(51) Chen, Y.; Chen, H.; Guo, L.; He, Q.; Chen, F.; Zhou, J.; Feng, J.; Shi, J. Hollow/Rattle-Type Mesoporous Nanostructures by a Structural Difference-Based Selective Etching Strategy. *ACS Nano* **2010**, *4*, 529−539.
(52) Rim, H. P.; Min, K. H.; Lee, H. J.; Jeong, S. Y.; Lee, S. C. Drug Delivery pH-Tunable Calcium Phosphate Covered Mesoporous Silica Nanocontainers for Intracellular Controlled Release of Guest Drugs. *Angew. Chem., Int. Ed.* **2011**, *50*, 8853−8857.

DOI: 10.1021/acsami.5b02146
ACS Appl. Mater. Interfaces 2015, 7, 10905−10914